NATURAL SCIENCE REVIEW 3 200804 (2026)
nsr.jinr.int

Radiation-induced surface smoothing and structural relaxation in electron-irradiated ZnS and ZnSe crystals

M. Yu. Tashmetov[1] and B. N. Madaminov*[1]

[1] *Institute of Nuclear Physics, Uzbekistan Academy of Sciences, Tashkent, Uzbekistan*

Abstract

The evolution of surface morphology and structural parameters in ZnS and ZnSe crystals under high-energy electron irradiation was investigated using a phenomenological modeling approach based on experimentally obtained irradiation-dependent structural and morphological data. The analysis focused on the fluence dependence of the surface roughness parameters R_a and R_z, coherent-domain size, and lattice parameter in the electron fluence range of $(0{-}2.5)\cdot 10^{17}$ electrons/cm^2. It was found that the surface roughness parameters R_a and R_z decrease according to an exponential law, indicating the occurrence of radiation-induced surface smoothing. A phenomenological kinetic equation describing roughness relaxation as a function of electron fluence was proposed and solved analytically. The obtained model demonstrates that the smoothing rate is proportional to the excess surface roughness relative to the limiting relaxed state. In contrast, the coherent-domain size generally increases with increasing fluence, whereas the lattice parameter decreases nearly linearly, indicating radiation-induced structural relaxation, lattice compaction, and defect rearrangement processes. Comparative analysis of ZnS and ZnSe crystals revealed differences in the smoothing kinetics and structural evolution parameters, which may be associated with differences in defect mobility and irradiation-assisted relaxation processes. Correlations were observed between the fluence-dependent evolution of surface roughness and bulk structural parameters, indicating concurrent morphological and structural changes under electron irradiation. The proposed phenomenological description provides a framework for comparing these irradiation-induced responses in ZnS and ZnSe crystals.

Keywords: ZnS crystal, ZnSe crystal, electron irradiation, surface smoothing, surface roughness, structural relaxation

DOI: 10.54546/NaturalSciRev.200804

1. Introduction

ZnS and ZnSe are important II–VI wide-bandgap semiconductor materials that attract considerable attention due to their optical, luminescent, and electronic properties. These materials are widely used in infrared optics, photodetectors, electroluminescent devices, phosphors, optical windows, and radiation-resistant optoelectronic systems [1–3]. ZnS possesses a relatively

*Corresponding author e-mail address: madaminov.b@inp.uz

Received: 17 June 2026; Revised: 14 August 2026; Accepted: 14 August 2026; Published: 11 September 2026

wide bandgap and high optical transparency in the visible spectral region, while ZnSe is characterized by high transparency in the infrared range and good optical performance for CO_2-laser applications [2, 3]. Owing to their favorable physical properties, ZnS and ZnSe crystals are considered promising materials for operation under extreme environmental conditions, including radiation exposure.

The structural and surface properties of ZnS and ZnSe crystals play a crucial role in determining their optical and mechanical performance. In particular, surface morphology, coherent-domain size, defect structure, and lattice stability significantly affect light scattering, optical absorption, and mechanical reliability of semiconductor devices [3, 4]. High-energy electron irradiation can modify these characteristics through the generation, migration, and recombination of radiation defects, leading to changes in crystal structure and surface state. Therefore, investigation of irradiation-induced structural and morphological evolution in ZnS and ZnSe crystals is of both fundamental and practical importance for the development of radiation-tolerant semiconductor and optical materials.

Numerous studies [5–8] have investigated the influence of irradiation on the structural, optical, and morphological properties of ZnS and ZnSe materials under various irradiation conditions. Electron, gamma, and ion irradiation were reported to induce lattice distortions, point defects, dislocation formation, and modifications of crystallinity in II–VI semiconductor compounds [5–8]. These radiation-induced processes strongly affect the lattice parameter, coherent-domain size, microstrain, and surface roughness of ZnS and ZnSe materials.

Particular attention has been devoted to the evolution of coherent-domain size and lattice parameters under irradiation. In ZnS thin films irradiated with high-energy electrons, a reduction in coherent-domain size accompanied by increased defect density and lattice disorder was observed, indicating significant irradiation-induced structural degradation [6]. Similar effects were reported for ZnSe thin films and nanostructures, where electron irradiation modified grain morphology, defect distribution, and local lattice strain through defect migration and recombination processes [7]. At sufficiently high irradiation doses, however, defect annihilation and radiation-stimulated diffusion may partially restore structural ordering, promoting coherent-domain enlargement and reduction of microstrain [8]. Such competing processes between defect generation and defect relaxation play an important role in determining the final structural state of irradiated semiconductor materials.

The lattice stability of ZnS and ZnSe under irradiation is also of considerable interest because lattice deformation directly influences the electronic band structure and phonon properties of these materials. Previous investigations [5, 8] demonstrated that electron irradiation can lead to contraction of the lattice parameter as a result of defect redistribution and relaxation of local elastic stresses. Such structural relaxation processes are commonly associated with the migration and recombination of Frenkel defects, vacancies, and interstitial atoms generated during electron–lattice interactions [9]. In addition, radiation-enhanced diffusion provides a physical basis for defect-assisted atomic redistribution in irradiated solids [10].

Surface morphology evolution under irradiation has been actively studied using atomic force microscopy (AFM). Several authors reported that irradiation can significantly modify the surface roughness and topography of ZnS and ZnSe crystals and films [5, 7, 8]. In particular, irradiation-induced defect migration and radiation-stimulated diffusion processes can enhance surface relaxation through atomic redistribution mechanisms, resulting in smoothing of surface asperities and a decrease in roughness parameters [10, 11]. This interpretation is also consistent with classical surface relaxation models, in which surface curvature and capillarity-driven atomic transport lead to gradual flattening of initially rough surfaces [12]. Such morphological changes are important because surface roughness strongly affects light scattering, optical transparency, and the functional stability of optical and semiconductor devices [13].

Recent studies have also demonstrated that structural and morphological modifications in ZnS and ZnSe are closely related to radiation-induced defect dynamics and electron–phonon interactions [8, 14]. Radiation-induced point defects can alter local lattice polarization, defect-related phonon scattering, and electron–phonon coupling processes, thereby influencing Raman spectra, optical absorption edge behavior, and Urbach energy [14, 15]. In addition, irradiation-induced defect evolution and surface morphology transformations are directly connected with changes in mechanical properties such as microhardness, fracture resistance, and structural stability [5, 8, 16].

Although considerable progress has been achieved in understanding irradiation effects in ZnS- and ZnSe-based materials, most previous studies have mainly focused on thin films, nanostructures, or optical characteristics separately. Comprehensive investigations combining surface morphology evolution, coherent-domain enlargement, lattice relaxation, and their mutual correlation in bulk ZnS and ZnSe crystals under high-fluence electron irradiation remain relatively limited. In particular, the relationship between irradiation-induced surface smoothing and bulk structural relaxation has not been systematically analyzed using a unified phenomenological approach.

Therefore, further investigation of the concurrent surface and structural transformations in electron-irradiated ZnS and ZnSe crystals is necessary for understanding their irradiation-induced evolution and relaxation behavior. Such studies are important for the development of radiation-resistant wide-bandgap semiconductor and optoelectronic materials operating under extreme irradiation environments.

2. Materials and methods

ZnS and ZnSe single crystals were used as the objects of investigation in this work. Bulk ZnS and ZnSe crystals were grown by the chemical vapor deposition (CVD) technique under optimized growth conditions described in previous studies [5, 8, 14]. The obtained crystals exhibited high structural quality and homogeneous morphology, making them suitable for investigations of irradiation-induced structural and surface transformations.

The crystals were irradiated with accelerated electrons using the “Elektronika U-003” electron accelerator at the Institute of Nuclear Physics, Academy of Sciences of the Republic of Uzbekistan [17, 18]. The electron energy was 2 MeV, while the irradiation fluence (Φ) varied in the range from 0 to $2.5 \cdot 10^{17}$ electrons/cm^2. The fluence values used in the experiments were $0.5 \cdot 10^{17}$, $1.0 \cdot 10^{17}$, $1.5 \cdot 10^{17}$, $2.0 \cdot 10^{17}$, and $2.5 \cdot 10^{17}$ electrons/cm^2. Irradiation was carried out at room temperature under atmospheric conditions.

The structural properties of the irradiated and non-irradiated crystals were investigated by X-ray diffraction (XRD) using a PANalytical Empyrean Series 3 diffractometer with CuK_α radiation. Diffraction patterns were recorded in the 2θ scanning mode at room temperature. The phase composition and structural parameters of the crystals were analyzed using the Rietveld refinement method implemented in the FullProf software package [19]. During the Rietveld refinement, the scale factor, background, zero shift, lattice parameter, site occupancies, preferred-orientation parameter, and profile/microstructural broadening parameters were refined.

The lattice parameter (a), coherent scattering domain size (D), and lattice microstrain (ε) were determined from the diffraction data, while an indirect dislocation-density estimate (δ) was subsequently calculated from D.

The instrumental contribution to diffraction-line broadening was determined using a LaB_6 standard reference material measured under identical instrumental conditions and was incorporated into FullProf as the instrumental resolution function. The diffraction profiles of the ZnS and ZnSe samples were subsequently refined over the whole 2θ range using the Thompson–Cox–Hastings (TCH) pseudo-Voigt profile function (Npr = 7) within an isotropic size–strain broadening model [19]. After accounting for the instrumental resolution function obtained from LaB_6, the sample-dependent size- and strain-related contributions were separated simultaneously during whole-pattern refinement according to their different angular dependences. For the size- and strain-related contributions, the corresponding Gaussian and Lorentzian components were combined within the TCH formalism to obtain the pseudo-Voigt FWHM H and mixing parameter η, from which the respective integral breadths β_{size} and β_{strain} were obtained. The volume-averaged coherent scattering domain size, D, was then estimated from the size-related integral breadth using the Debye–Scherrer relation [20, 21],

$$D = \frac{K\lambda}{\beta_{\text{size}} \cos\theta}, \tag{1}$$

where K is the Scherrer constant, λ is the X-ray wavelength, β_{size} is the integral breadth of the size-related diffraction-line broadening component obtained from the TCH pseudo-Voigt profile after instrumental correction and size–strain separation, and θ is the Bragg diffraction angle.

An indirect estimate of the dislocation density, δ, was calculated from the coherent-domain size according to [22]

$$\delta = \frac{1}{D^2}, \tag{2}$$

while the lattice microstrain ε was determined from the separately resolved strain-related integral breadth (β_{strain}) using the Stokes–Wilson equation [23]

$$\varepsilon = \frac{\beta_{\text{strain}}}{4\tan\theta}. \tag{3}$$

Because δ is derived solely from D through Eq. (2), it should be regarded as a size-derived dislocation-density estimate rather than as an independently measured dislocation density. This relation does not account for the spatial distribution, configuration, or possible rearrangement of dislocations. The obtained microstrain ε represents a volume-averaged measure of local lattice distortions associated with elastic strain fields arising from dislocations and other crystal defects.

The lattice parameter a for the cubic structure was determined from the interplanar spacing relation

$$a = d\sqrt{h^2 + k^2 + l^2}, \tag{4}$$

where d is the interplanar spacing and h, k, and l are the Miller indices of the corresponding diffraction plane.

The surface morphology of the crystals before and after irradiation was studied using a Shimadzu SPM-9700HT atomic force microscope. For the AFM investigation, the same specimen was used throughout the irradiation experiment. The surface morphology of the non-irradiated specimen was first characterized by AFM. The specimen was then successively irradiated with 2 MeV electrons to cumulative fluences of $0.5{\cdot}10^{17}$, $1.0{\cdot}10^{17}$, $1.5{\cdot}10^{17}$, $2.0{\cdot}10^{17}$, and $2.5{\cdot}10^{17}$ electrons/cm^2. After each irradiation step, AFM measurements were performed on the same specimen to monitor the progressive evolution of the surface morphology. AFM images were recorded at room temperature with a scan area of $30 \times 30\ \mu\mathrm{m}^2$. The average surface roughness (R_a) and maximum profile height roughness (R_z) were extracted from the AFM topography images using the standard software package supplied with the microscope. The evolution of the surface morphology with increasing electron fluence was analyzed comparatively for ZnS and ZnSe crystals.

The experimentally obtained fluence dependences of the surface roughness parameters were analyzed using a phenomenological relaxation model. Since the AFM results demonstrated a gradual saturation behavior of the roughness parameters with increasing electron fluence, the surface smoothing process was considered within the framework of a first-order kinetic relaxation approach.

The fluence dependences of the coherent-domain size and lattice parameter were analyzed with linear and nonlinear regression models. In particular, the roughness parameters were fitted using an exponential relaxation function, while the structural parameters were analyzed applying polynomial and linear approximation models. Numerical fitting and statistical analysis of the experimental data were performed with Wolfram Mathematica and Origin software packages. The quality of the fitting models was evaluated using the coefficient of determination (R^2) and residual analysis.

3. Results

3.1. Evolution of surface morphology under electron irradiation

Figures 1 and 2 show the three-dimensional AFM surface topography images of ZnS and ZnSe crystals irradiated with electron fluences ranging from 0 to $2.5 \cdot 10^{17}$ electrons/cm^2. For both materials, the AFM images reveal progressive surface smoothing, manifested by a reduction in surface relief amplitude and suppression of high-curvature topographic features with increasing electron fluence.

For the non-irradiated ZnS crystal, the AFM images reveal a morphologically heterogeneous surface characterized by pronounced surface asperities, irregular height distribution, and large-amplitude topographic inhomogeneities. As the electron fluence increases, both the height and

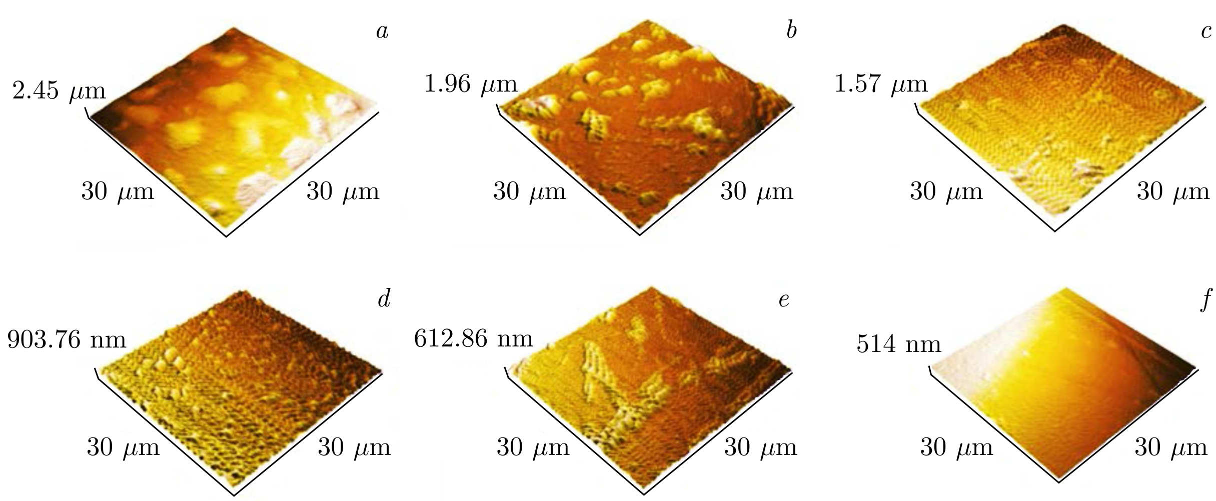

Figure 1. Three-dimensional AFM images of the ZnS crystal surface: *a*) non-irradiated; *b*) irradiated with electron fluences of $0.5{\cdot}10^{17}$, $1.0{\cdot}10^{17}$ (*c*), $1.5{\cdot}10^{17}$ (*d*), $2.0{\cdot}10^{17}$ (*e*) and $2.5{\cdot}10^{17}$ electrons/cm^2 (*f*).

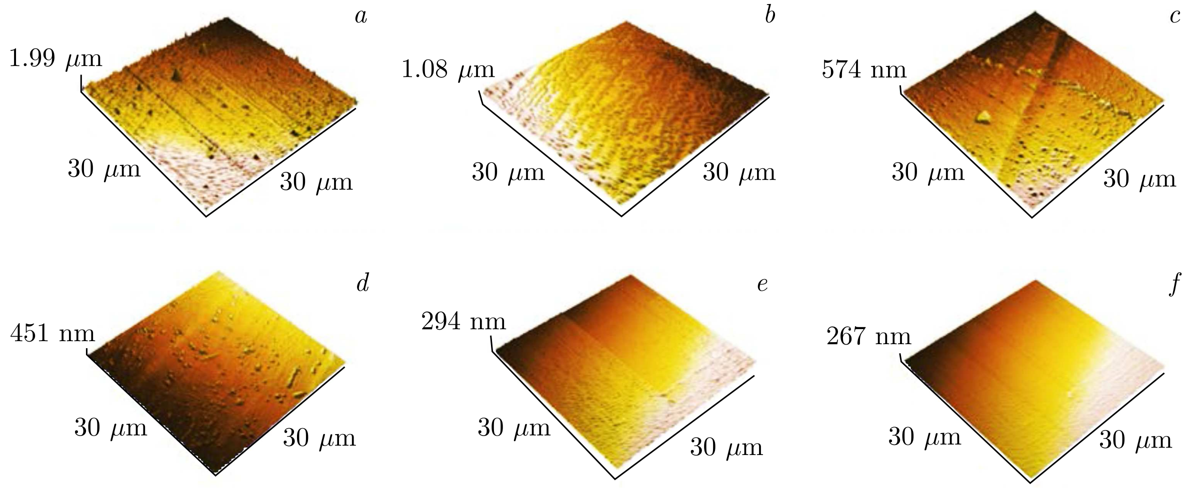

Figure 2. Three-dimensional AFM images of the ZnSe crystal surface: *a*) non-irradiated; *b*) irradiated with electron fluences of $0.5{\cdot}10^{17}$, $1.0{\cdot}10^{17}$ (*c*), $1.5{\cdot}10^{17}$ (*d*), $2.0{\cdot}10^{17}$ (*e*) and $2.5{\cdot}10^{17}$ electrons/cm^2 (*f*).

density of surface irregularities decrease significantly. At fluences of $1.5 \cdot 10^{17}$ and $2.0 \cdot 10^{17}$ electrons/cm^2, the surface becomes noticeably smoother, while at $2.5{\cdot}10^{17}$ electrons/cm^2 a relatively homogeneous and flattened surface morphology is observed.

The same qualitative evolution is observed for ZnSe crystals (Figure 2). Compared with the non-irradiated state, electron irradiation progressively suppresses prominent surface features, resulting in a more homogeneous surface topography at higher electron fluences.

The qualitative changes observed in the AFM images indicate a progressive evolution of the surface morphology with increasing electron fluence. To quantify these changes, the average roughness (R_a) and maximum roughness height (R_z) parameters were analyzed as a function of electron fluence, as presented in the following section.

3.2. Fluence dependence of roughness parameters

To quantitatively characterize the irradiation-induced evolution of the surface morphology, the fluence dependences of the roughness parameters R_a and R_z were analyzed for ZnS and ZnSe crystals. Figure 3 presents the experimental data together with the corresponding phenomenological fitting curves. For both materials, the roughness parameters decrease monotonically with increasing electron fluence and exhibit a pronounced non-linear behavior approaching saturation at higher fluences.

For ZnS crystals, the R_a parameter decreases from 191 nm for the non-irradiated sample to 34 nm at a fluence of $2.5 \cdot 10^{17}$ electrons/cm^2, corresponding to a reduction by approximately 5.6 times. For ZnSe crystals, R_a decreases from 168 to 21 nm, corresponding to an approximately 8-fold reduction over the same fluence range. These results indicate that the reduction of the average surface roughness is more pronounced in ZnSe than in ZnS.

The maximum roughness height parameter R_z exhibits a similar evolution with increasing electron fluence. For ZnS crystals, R_z decreases from 1929 to 399 nm, whereas for ZnSe crystals it decreases from 1628 to 219 nm between 0 and $2.5{\cdot}10^{17}$ electrons/cm^2. Compared with R_a, the reduction of R_z is more pronounced, particularly at low and intermediate irradiation fluences.

To quantitatively describe the experimentally observed relaxation behavior, the fluence dependences of the roughness parameters were approximated using an exponential saturation

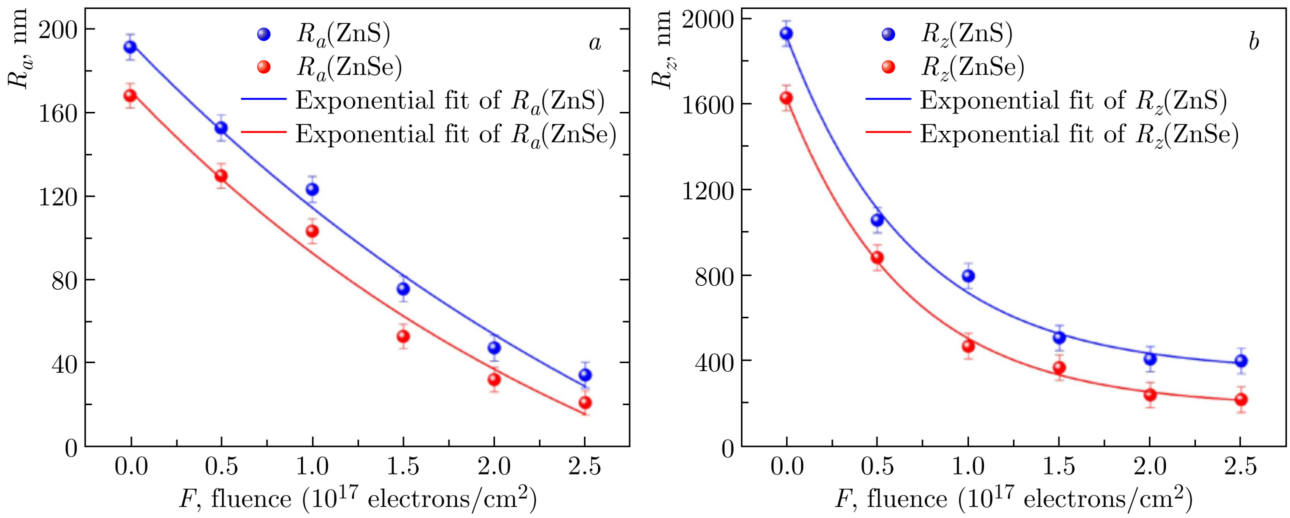

Figure 3. Fluence dependences of the surface roughness parameters R_a (*a*) and R_z (*b*) for ZnS and ZnSe crystals under electron irradiation. Symbols represent the experimental data, while solid curves correspond to the results of exponential fitting.

function derived from the phenomenological model:

$$R(F) = R_\infty + Ae^{-kF}, \tag{5}$$

where $F = \Phi/(10^{17}\,\text{electrons/cm}^2)$ is the normalized electron fluence, R_∞ is the limiting roughness value corresponding to the relaxed surface state, A is the relaxation amplitude ($A = R_0 - R_\infty$), and k is the exponential relaxation coefficient characterizing the efficiency of irradiation-induced surface smoothing.

The fitting results demonstrate excellent agreement between the phenomenological model and the experimental data. For ZnS crystals, fitting of the $R_a(F)$ dependence yielded $R^2 = 0.990$, while for ZnSe $R^2 = 0.984$. Similarly, the $R_z(F)$ dependences showed even better agreement with the exponential relaxation model, with $R^2 = 0.994$ for ZnS and $R^2 = 0.998$ for ZnSe. The corresponding fitting parameters, including the limiting roughness R_∞, relaxation amplitude A, and smoothing coefficient k, are summarized in Table 1. The high coefficients of determination indicate that the proposed phenomenological model provides an excellent description of the experimentally observed roughness evolution within the investigated fluence range.

The experimental dependences of $R_a(F)$ and $R_z(F)$ are therefore well described by the proposed phenomenological exponential relaxation model.

Table 1. Exponential fitting parameters for the fluence dependences of the roughness parameters $R_a(F)$ and $R_z(F)$ in ZnS and ZnSe crystals according to Eq. (5).

Crystal	Parameter	R_∞, nm	A, nm	k	R^2
ZnS	$R_a(F)$	28.4	162.60	0.82	0.990
ZnSe	$R_a(F)$	17.9	150.10	0.96	0.984
ZnS	$R_z(F)$	347.6	1570.66	1.45	0.994
ZnSe	$R_z(F)$	183.7	1447.23	1.51	0.998

3.3. Irradiation-induced structural and microstructural evolution

Figure 4 shows the X-ray diffraction patterns of non-irradiated and electron-irradiated ZnS and ZnSe crystals at the maximum investigated fluence of $2.5 \cdot 10^{17}$ electrons/cm^2. For both crystals, the diffraction patterns confirm preservation of the cubic crystal structure (space group F–43m) after electron irradiation.

For a more detailed analysis of the structural state of the non-irradiated and electron-irradiated ZnS and ZnSe crystals, full-profile Rietveld refinements of the X-ray diffraction patterns were performed using the FullProf software package. Figure 4 also presents the experimental diffraction profiles, calculated patterns, difference curves ($Y_{\text{obs}} - Y_{\text{calc}}$), and Bragg reflection positions for ZnS and ZnSe crystals before and after electron irradiation with a fluence of $2.5 \cdot 10^{17}$ electrons/cm^2. As can be seen from Figure 4, the calculated profiles reproduce the experimental diffraction patterns well for both materials. The absence of additional diffraction peaks confirms the preservation of the cubic crystal structure of ZnS and ZnSe after electron irradiation.

The agreement factors obtained from the refinements are at an acceptable level. For the non-irradiated and irradiated ZnS crystals, the corresponding values are $R_B = 3.27$ and 3.83%,

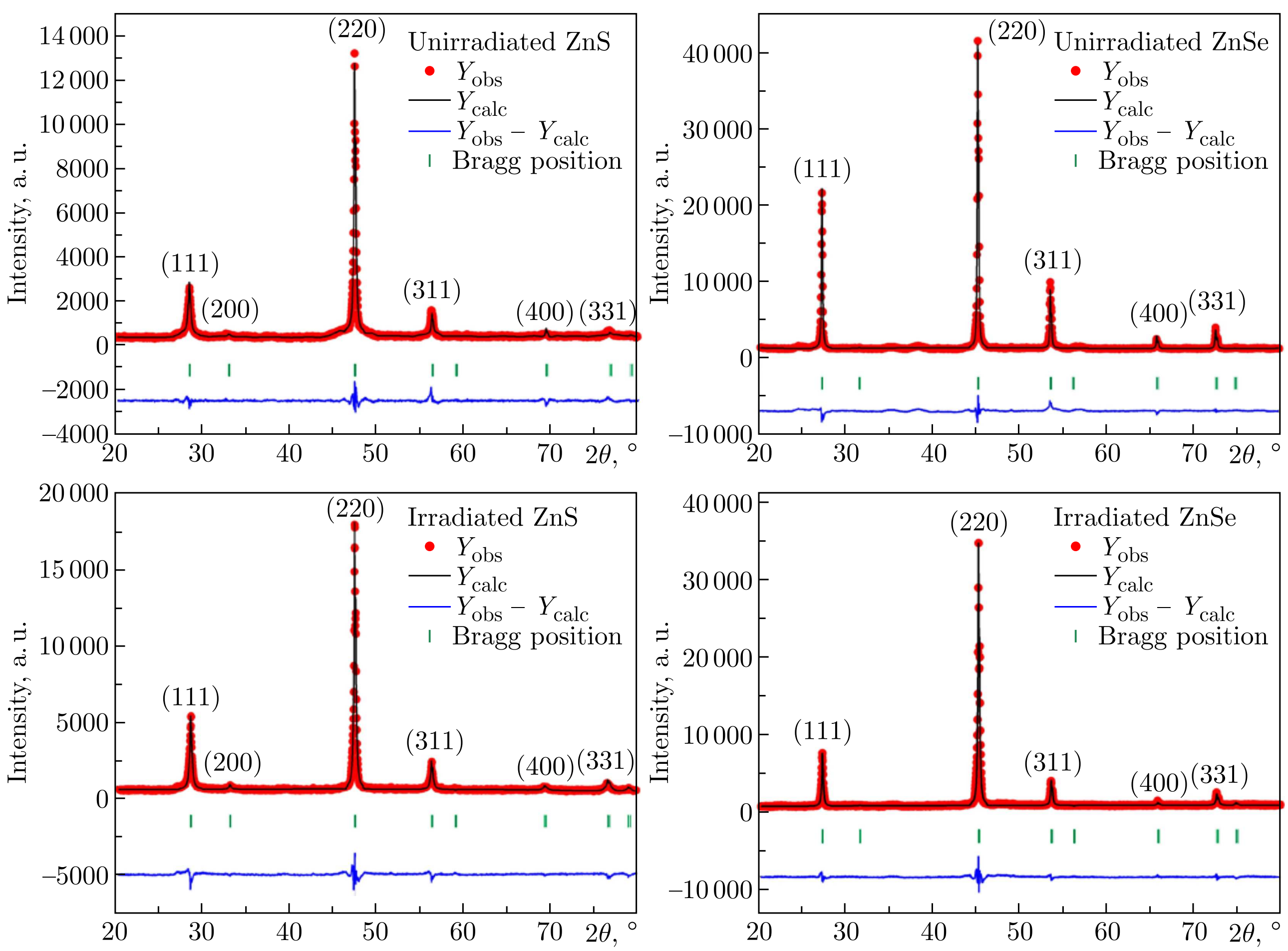

Figure 4. X-ray diffraction patterns of ZnS and ZnSe crystals before and after electron irradiation with a fluence of $2.5 \cdot 10^{17}$ electrons/cm^2. Red symbols correspond to the experimental data (Y_{obs}), black lines represent the calculated profiles (Y_{calc}), blue lines show the difference curves ($Y_{\text{obs}} - Y_{\text{calc}}$), and vertical ticks indicate the positions of the Bragg reflections.

$R_F = 2.26$ and 4.28%, and $\chi^2 = 3.68$ and 3.21, respectively. For ZnSe, the corresponding values are $R_B = 3.94$ and 2.90%, $R_F = 5.07$ and 4.24%, and $\chi^2 = 2.07$ and 2.31. These results confirm the satisfactory quality of the Rietveld refinements and the reliability of the determined structural parameters.

At the same time, slight shifts and modifications of the diffraction peak shapes are observed after irradiation [5, 8], indicating changes in the structural state of the crystals. The observed evolution of the diffraction peaks suggests irradiation-induced lattice relaxation and modification of the microstructural parameters, including coherent-domain size and local lattice strain [5, 8].

The decrease in the FWHM of the (111) reflection with increasing fluence indicates a reduction in the overall diffraction-line broadening, consistent with the coherent-domain enlargement and reduced lattice microstrain obtained from the whole-pattern analysis [5, 8, 14].

Slight variations in the relative diffraction peak intensities are observed after electron irradiation. However, no additional diffraction peaks are detected, and all reflections remain indexed to the cubic zinc-blende structure, indicating preservation of the crystalline phase throughout the investigated fluence range. The relative intensities were accounted for within the whole-pattern Rietveld refinement through the refined structural and profile parameters, including site occupancies and preferred orientation. The microscopic origin of these small intensity variations cannot be uniquely determined from the present XRD data alone.

In addition to surface morphology modification, electron irradiation also affects the structural parameters of ZnS and ZnSe crystals. The evolution of the lattice parameter (a) and coherent-domain size (D) as a function of electron fluence was analyzed in order to clarify the relationship between surface smoothing and bulk structural relaxation. The fluence dependences of the a and D for ZnS and ZnSe crystals are presented in Figure 5.

For ZnS crystals, the lattice parameter decreases from 0.54413 nm in the non-irradiated state to 0.54256 nm at a fluence of $1.5 \cdot 10^{17}$ electrons/cm^2 (Figure 5, *a*). At higher fluences, a slight increase to approximately 0.54305–0.54306 nm is observed. Such a behavior suggests that the initial stage of irradiation is dominated by lattice contraction associated with formation and redistribution of radiation-induced point defects. At higher fluences, competing relaxation processes including defect migration, recombination, and partial release of local elastic stresses may lead to weak recovery of the lattice parameter. For ZnSe crystals, the lattice parameter decreases more monotonically from 0.56863 to 0.56811 nm as the electron fluence increases from 0 to $2.5 \cdot 10^{17}$ electrons/cm^2. The observed decrease in the lattice parameter indicates radiation-induced lattice compaction, which may be associated with defect redistribution, local structural relaxation, and suppression of nonequilibrium lattice distortions.

The coherent-domain size also changes under electron irradiation, as shown in Figure 5, *b*. In ZnS crystals, the coherent-domain size increases from 19.88 nm in the non-irradiated state to 26.68 nm at $2.5 \cdot 10^{17}$ electrons/cm^2. Although the intermediate values exhibit weak non-monotonic behavior, the overall tendency indicates irradiation-assisted coherent-domain enlargement. This behavior is consistent with irradiation-assisted defect rearrangement, improved structural coherence, and reduction of microstructural fragmentation. In ZnSe crystals, the coherent-domain size increases more systematically from 32.00 to 37.03 nm over the same fluence range. The more monotonic evolution of D in ZnSe suggests a more regular irradiation-induced structural response compared with ZnS. The increase in coherent-domain size may be associated with irradiation-assisted defect redistribution and a reduction in microstructural disorder.

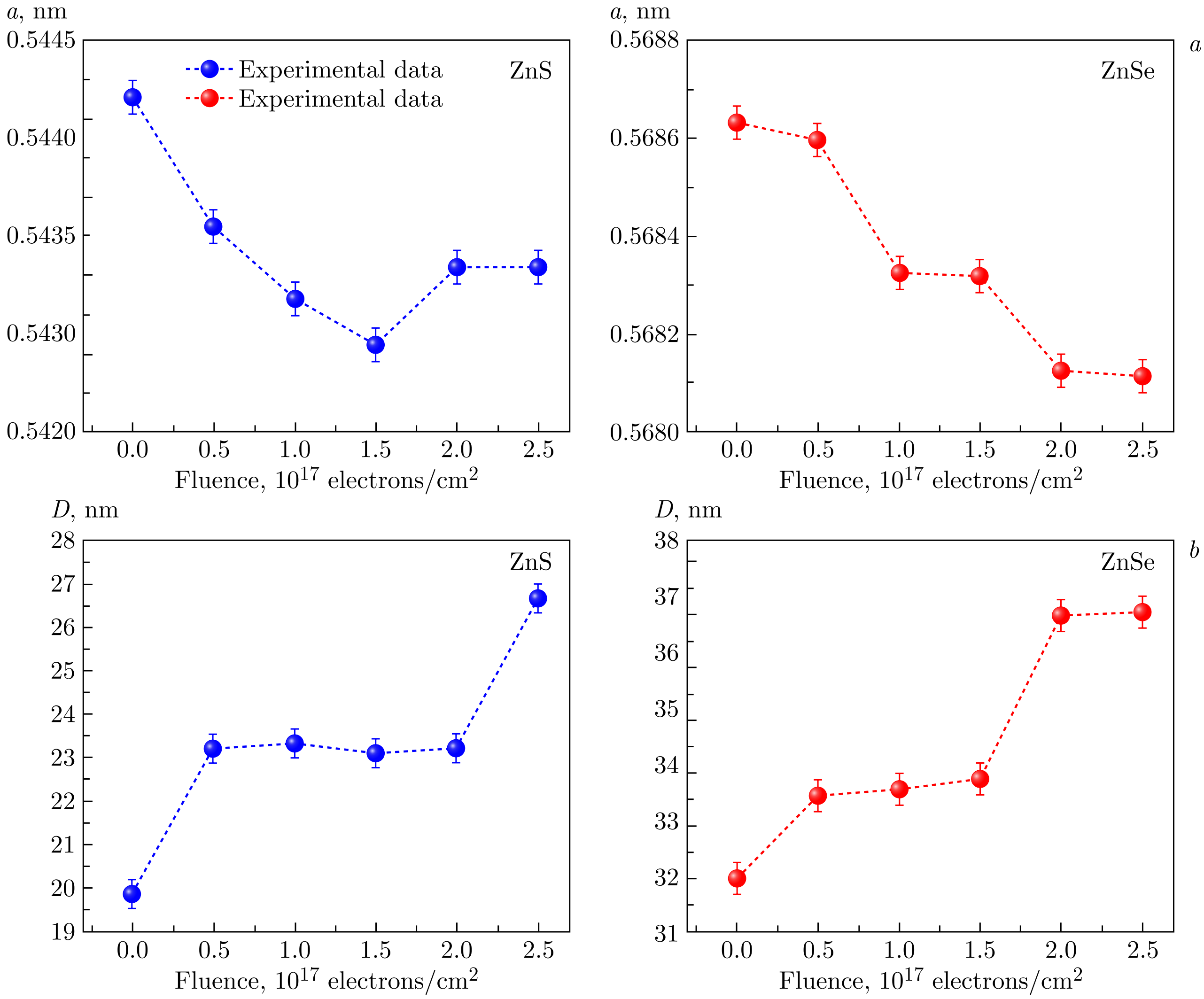

Figure 5. Fluence dependences of the lattice parameter (a) and the coherent-domain size (b) for ZnS and ZnSe crystals under electron irradiation. The decrease in the lattice parameter indicates radiation-induced lattice compaction and structural relaxation, whereas the increase in coherent-domain size reflects irradiation-assisted coherent-domain enlargement and microstructural ordering.

The simultaneous decrease in the lattice parameter and increase in coherent-domain size indicate that electron irradiation does not simply induce structural disorder in ZnS and ZnSe crystals. Instead, within the investigated fluence range, irradiation activates competing nonequilibrium processes: generation of radiation defects on the one hand, and defect migration, recombination, and structural relaxation on the other. The dominance of relaxation-related processes at high fluences can promote lattice compaction, reduction of local strain fields, and enlargement of coherent scattering regions. These results demonstrate the dual role of high-energy electron irradiation as both a source of lattice defects and a driving force for irradiation-assisted structural relaxation.

The structural relaxation process is accompanied by an increase in coherent-domain size and a decrease in lattice microstrain (ε) under electron irradiation up to a fluence of $2.5 \cdot 10^{17}$ electrons/cm^2. The size-derived dislocation-density estimate (δ), calculated using Eq. (2), decreases from $25.3 \cdot 10^{10}$ to $14.05 \cdot 10^{10}$ cm^{-2} in ZnS and from $9.77 \cdot 10^{10}$ to $7.29 \cdot 10^{10}$ cm^{-2} in ZnSe. Since δ is derived directly from D, its evolution reflects the corresponding change in coherent-domain size rather than an independent determination of the dislocation density. At the same time, the microstrain decreases from $7.11 \cdot 10^{-3}$ to $5.29 \cdot 10^{-3}$ in ZnS and from $4.62 \cdot 10^{-3}$ to $3.99 \cdot 10^{-3}$ in ZnSe. The concurrent evolution of coherent-domain size and microstrain is consistent with a reduction of microstructural distortions and possible rearrangement of the defect and dislocation structure under irradiation. These structural changes are consistent with irradiation-assisted defect migration and relaxation processes in the crystal lattice.

These structural changes occur concurrently with the observed surface-morphology evolution: the reduction in surface roughness is accompanied by coherent-domain enlargement and changes in the lattice parameter, indicating correlated morphological and structural evolution under electron irradiation.

3.4. Correlation between surface and structural evolution

To clarify the relationship between surface morphology evolution and bulk structural modifications, correlation analysis between the roughness parameters (R_a, R_z) and the structural parameters (D, a) was performed for ZnS and ZnSe crystals. The obtained results reveal systematic correlations between the fluence-dependent evolution of surface roughness and the structural parameters of both crystals.

Figure 6 shows the dependences of the average surface roughness parameter R_a on coherent-domain size (D) and lattice parameter (a) for ZnS and ZnSe crystals. For both ZnS and ZnSe crystals, the reduction of R_a is accompanied by an increase in coherent-domain size (Figure 6, *a*). This behavior indicates that irradiation-induced surface smoothing occurs simultaneously with enlargement of coherent scattering domains and partial structural ordering of the crystal lattice. The obtained relationship indicates that surface smoothing proceeds concurrently with enlargement of coherent scattering domains as the electron fluence increases.

In ZnS crystals, the increase in coherent-domain size from approximately 20 to 27 nm is accompanied by a significant decrease in R_a from 191 to 34 nm. A similar tendency is observed for ZnSe crystals, where the coherent-domain size increases from 32 to 37 nm while the roughness decreases from 168 to 21 nm. The observed trend is consistent with irradiation-induced microstructural relaxation and enlargement of coherent scattering regions. The simultaneous re-

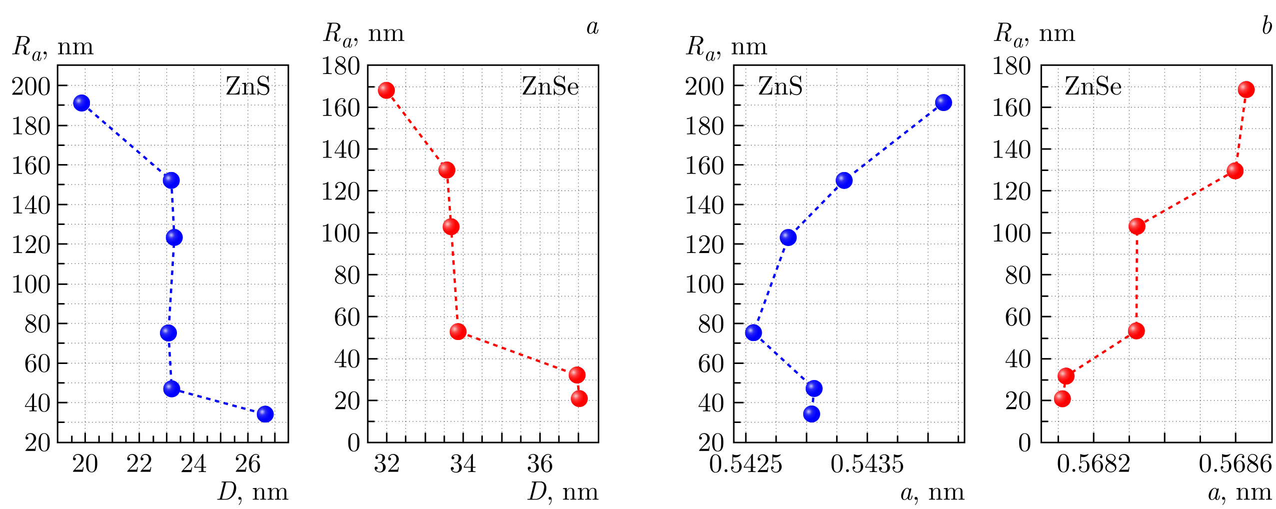

Figure 6. Dependences of the average surface roughness parameter R_a on coherent-domain size (*a*) and lattice parameter (*b*) for ZnS and ZnSe crystals. The observed correlations illustrate the concurrent evolution of surface roughness and structural parameters under electron irradiation.

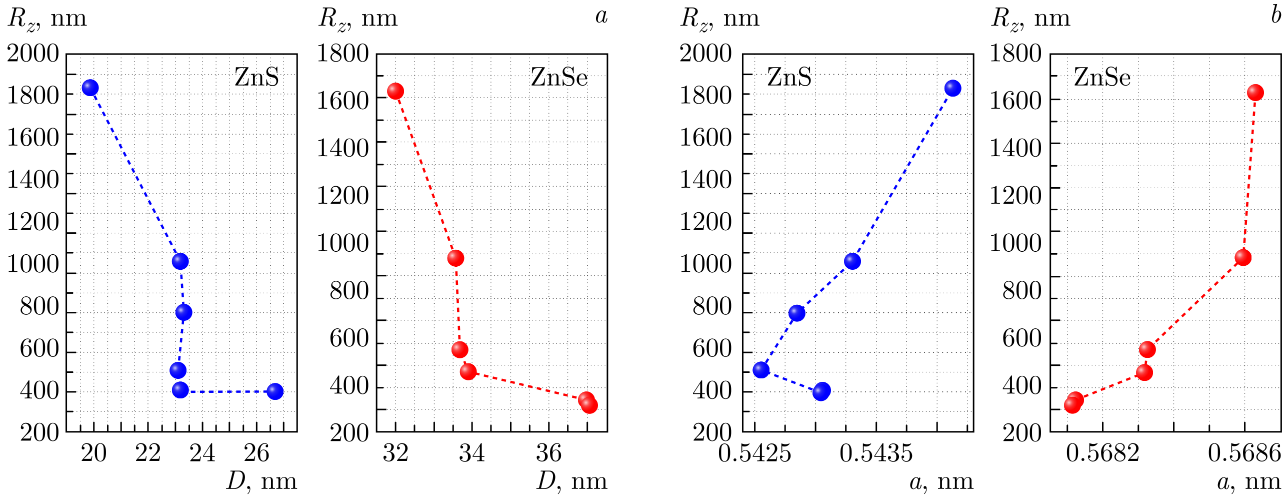

Figure 7. Dependences of the maximum roughness height parameter R_z on coherent-domain size D (a) and lattice parameter a (b) for ZnS and ZnSe crystals.

duction in surface roughness indicates that the morphological and structural parameters evolve in parallel with increasing fluence.

Figure 6*b* presents the dependence of the roughness parameter R_a on the lattice parameter (a). It can be seen that the decrease in surface roughness is accompanied by gradual reduction of the lattice parameter for both crystals. This tendency shows that the reduction in surface roughness occurs concurrently with the irradiation-induced changes in the lattice parameter. The reduction of the lattice parameter may result from redistribution and partial annihilation of radiation-induced point defects, leading to relaxation of local elastic strain fields within the crystal lattice.

A similar tendency is also observed for the R_z parameter, as shown in Figures 7, *a* and 7, *b*, which present the dependences of R_z on coherent-domain size and lattice parameter. The decrease in R_z with increasing coherent-domain size and decreasing lattice parameter are consistent with the preferential suppression of large-amplitude surface asperities and highly nonequilibrium topographic defects. Since R_z is particularly sensitive to isolated large surface features and maximum height variations of the surface profile, the obtained behavior indicates that large-amplitude surface irregularities relax more efficiently during the initial stages of irradiation-assisted structural evolution.

The obtained relationships demonstrate that surface morphology and structural parameters evolve concurrently under electron irradiation. The simultaneous decrease in surface roughness, increase in coherent-domain size, and change in lattice parameter reveal a consistent fluence-dependent correlation between the morphological and structural responses of both ZnS and ZnSe crystals. These correlations provide a useful phenomenological basis for considering the surface and bulk evolution together, without implying a direct causal relationship between them.

4. Discussion

4.1. Phenomenological model of radiation-induced surface smoothing

The AFM results demonstrate that high-energy electron irradiation induces a pronounced reduction of the surface roughness parameters R_a and R_z in both ZnS and ZnSe crystals. The experimentally observed roughness evolution exhibits a distinctly non-linear behavior: rapid smoothing occurs at the initial stage of irradiation, whereas at higher fluences the relaxation process gradually slows down and approaches a saturation-like regime. Such behavior is characteristic of nonequilibrium relaxation processes in which the driving force decreases progressively as the system approaches a more energetically stable surface state. Similar relaxation-type surface evolution has previously been reported for irradiation-assisted surface smoothing and capillarity-driven relaxation processes in irradiated materials [10–12].

The AFM images (Figs. 1 and 2) provide additional qualitative evidence for this behavior. During the early stages of irradiation, the most pronounced surface asperities are preferentially suppressed, whereas at higher fluences the remaining topographic irregularities become progressively smaller and more uniformly distributed. This observation is fully consistent with the quantitative evolution of the roughness parameters. In particular, the larger reduction of R_z compared with R_a indicates that electron irradiation preferentially eliminates high-amplitude surface features before affecting the average surface roughness. Since R_z is considerably more sensitive than R_a to isolated peaks and valleys, its faster relaxation suggests a progressive reduction of the highest-energy morphological features of the surface.

To describe the observed smoothing behavior quantitatively, the irradiation-induced relaxation process is represented by a phenomenological kinetic model in which the electron fluence serves as the external parameter governing the evolution of the surface morphology. Assuming that the relaxation rate is proportional to the remaining excess roughness of the nonequilibrium surface leads to the first-order kinetic equation

$$\frac{dR}{dF} = -k(R - R_\infty), \tag{6}$$

where R represents the roughness parameter (R_a or R_z), F is the normalized electron fluence, k is the phenomenological relaxation coefficient, and R_∞ represents the limiting roughness corresponding to the relaxed surface state.

According to Eq. (6), the relaxation rate naturally decreases as the surface approaches its limiting morphology. At low electron fluences, where the excess roughness $R - R_\infty$ is large, smoothing proceeds rapidly. As irradiation continues, progressively fewer high-amplitude surface features remain, resulting in slower relaxation kinetics and gradual saturation of the roughness evolution.

Equation (6) can be solved analytically by separating the variables:

$$\frac{dR}{(R - R_\infty)} = -kdF.$$

Integration gives

$$\ln|R - R_\infty| = -kF + C,$$

where C is the integration constant. Applying the initial condition $R = R_0$ at $F = 0$, where R_0 is the roughness of the non-irradiated crystal, gives the final expression

$$R(F) = R_\infty + (R_0 - R_\infty)\, e^{-kF}. \tag{7}$$

This expression represents a saturating exponential relaxation law for irradiation-induced surface smoothing. Here, $R_0 - R_\infty$ is the initial excess roughness that can be relaxed under irradiation, while k characterizes the efficiency of the smoothing process. The obtained solution describes a saturation-type relaxation process in which the roughness decreases rapidly at low fluences and gradually approaches a limiting value at higher irradiation fluences.

For practical fitting of the experimental data, Eq. (7) can also be written in the form commonly used in Origin software:

$$R(F) = y_0 + Ae^{-kF}, \tag{8}$$

where $y_0 \equiv R_\infty$ and $A \equiv R_0 - R_\infty$.

The obtained fitting parameters (Table 1) provide additional quantitative support for the proposed phenomenological description. For both ZnS and ZnSe, the relaxation coefficients determined for R_z are consistently higher than those obtained for R_a, indicating that high-amplitude surface irregularities relax more rapidly than the average surface roughness. This conclusion agrees well with the AFM observations, which show preferential suppression of the largest asperities during the early stages of irradiation. Moreover, the excellent agreement between the experimental data and Eq. (7), reflected by the high coefficients of determination ($R^2 = 0.984{-}0.998$), demonstrates that the exponential relaxation law provides an adequate phenomenological description of the observed surface evolution over the investigated fluence range.

The physical interpretation of this behavior is consistent with irradiation-induced defect processes occurring in the near-surface region. High-energy electrons generate nonequilibrium point defects, primarily vacancies and interstitial atoms, whose redistribution enhances local atomic mobility. Under these conditions, surface regions possessing higher local curvature and excess surface energy relax preferentially through irradiation-assisted atomic rearrangement, resulting in progressive suppression of large surface asperities and subsequent reduction of the overall surface roughness [10–12]. The experimentally observed evolution of R_a and R_z is therefore consistent with a defect-mediated surface relaxation process. However, the present work does not directly observe atomic-scale defect migration; consequently, this interpretation should be regarded as being supported by the observed experimental correlations rather than as direct experimental proof of the underlying microscopic mechanism.

It should be emphasized that the phenomenological relaxation coefficient k is a fitting parameter describing the rate at which the surface roughness approaches its limiting value with increasing electron fluence. It should not be interpreted as a diffusion coefficient or a direct measure of defect mobility. Instead, k provides a convenient phenomenological parameter for comparing the relative efficiency of irradiation-induced surface relaxation under identical irradiation conditions.

Finally, the proposed model has been validated only within the investigated electron fluence range of $(0{-}2.5) \cdot 10^{17}$ electrons/cm^2. Although Eq. (7) accurately reproduces the experimental observations within this interval, its applicability at substantially higher fluences has not been verified. Under more intense irradiation, additional processes, including accumulation of complex defect clusters, enhanced lattice damage, or changes in the dominant relaxation mechanisms, may become significant. Therefore, the present model should be regarded as a phenomenological description applicable to the investigated irradiation conditions rather than as a universal model for arbitrary electron fluences.

4.2. Radiation-stimulated defect dynamics and structural relaxation

The structural evolution of ZnS and ZnSe crystals under 2-MeV electron irradiation reflects the competition between radiation-induced defect generation and subsequent defect-assisted relaxation processes. Elastic collisions between energetic electrons and lattice atoms produce nonequilibrium point defects, including vacancies, interstitial atoms, and Frenkel pairs [9, 16, 24]. These defects locally distort the crystal lattice and modify the structural state of both the bulk and near-surface regions. As the electron fluence increases, however, the accumulated defect population also provides conditions for enhanced defect redistribution and partial defect annihilation, gradually driving the crystal toward a lower-energy structural configuration.

It should be emphasized that the present interpretation is based on experimentally observed structural correlations rather than on direct observation of defect migration. No *in situ* measurements of defect diffusion or atomic-scale defect evolution were performed in this work. Therefore, the proposed radiation-assisted relaxation mechanism should be regarded as a physically consistent interpretation supported by the combined evolution of the structural and morphological parameters together with previous studies of irradiated II–VI semiconductors [5, 8, 25].

The X-ray diffraction results provide quantitative evidence of progressive structural relaxation. For both ZnS and ZnSe, the lattice parameter decreases systematically with increasing electron fluence, from 0.54413 to approximately 0.54305 nm for ZnS and from 0.56863 to 0.56811 nm for ZnSe. The monotonic character of this evolution suggests gradual relaxation of irradiation-induced lattice distortions rather than random accumulation of structural disorder. Such behavior is consistent with partial redistribution and annihilation of metastable defect configurations, leading to reduction of local elastic strain fields [6–8].

Simultaneously, the coherent-domain size increases from approximately 20 to 27 nm in ZnS and from 32 to 37 nm in ZnSe. Since the coherent-domain size represents the average dimension of coherent scattering domains, its increase indicates improved structural coherence within the irradiated crystals. Rather than implying formation of new grains, this evolution suggests partial recovery of defect-rich regions and reduction of internal lattice fragmentation, resulting in larger coherent diffraction domains. Similar irradiation-assisted increases in coherent domain size have been reported for irradiated semiconductor materials undergoing defect relaxation [10, 26–28].

The concurrent decrease in lattice parameter and increase in coherent-domain size are mutually consistent with the structural evolution observed in the present study. Although these quantities characterize different aspects of the crystal structure, both evolve monotonically with electron fluence and indicate progressive reduction of the nonequilibrium state. Together with the decrease in lattice microstrain discussed in Section 3.3, these trends suggest that structural relaxation gradually becomes more significant as irradiation proceeds. It should be noted, however, that the estimated dislocation density and lattice microstrain are correlated descriptors of defect-induced lattice distortion and therefore should not be interpreted as completely independent evidence of structural relaxation.

The electron energy was fixed at 2 MeV throughout the present study in order to investigate the fluence-dependent structural and surface evolution under unchanged electron-transport conditions. According to the NIST ESTAR database, the CSDA range provides an estimate of the average path length traveled by electrons as they lose their energy in a material [29]. Thus, the selected electron energy enables substantial energy deposition within the bulk of the investigated ZnS and ZnSe crystals rather than restricting the irradiation effect exclusively to the near-surface region. At other electron energies, the electron range and energy-deposition profile would differ, potentially affecting the spatial distribution of irradiation-induced defects and the resulting structural and morphological evolution.

Comparison of the two materials reveals that ZnSe exhibits a more uniform evolution of both lattice parameter and coherent-domain size together with a higher relaxation coefficient obtained from the surface-smoothing model (Section 4.1). Although the present experiments do not directly determine defect mobility, this combination of structural and morphological observations suggests that irradiation-assisted relaxation proceeds somewhat more efficiently in ZnSe than in ZnS under identical irradiation conditions. Such differences may originate from variations in bonding characteristics, defect formation energies, and defect migration behavior between the two II–VI semiconductors.

Overall, the structural results indicate that, within the investigated fluence range, electron irradiation does not lead to continuous accumulation of structural disorder. Instead, the experimental observations are consistent with the coexistence of two competing nonequilibrium processes: continuous generation of radiation defects and simultaneous irradiation-assisted structural relaxation. The balance between these processes results in progressive reduction of lattice distortion, enlargement of coherent scattering domains, and increasing structural equilibration as the electron fluence increases.

4.3. Comparative analysis of ZnS and ZnSe crystals

Although ZnS and ZnSe exhibit the same overall irradiation-induced tendency toward surface smoothing and structural relaxation, the magnitude and regularity of these changes differ between the two materials. A direct comparison of the experimental data shows that ZnSe undergoes a more pronounced morphological response within the investigated fluence range.

The difference is particularly evident in the AFM roughness parameters. At a fluence of $2.5 \cdot 10^{17}$ electrons/cm^2, R_a decreases from 191 to 34 nm in ZnS, corresponding to a reduction of approximately 82%, whereas in ZnSe it decreases from 168 to 21 nm, corresponding to approximately 88%. Similarly, R_z decreases from 1929 to 399 nm in ZnS (approximately 79%) and from 1628 to 219 nm in ZnSe (approximately 87%). Thus, both the average roughness and the large-amplitude topographic irregularities are suppressed more strongly in ZnSe under identical irradiation conditions.

The fitting parameters provide an additional quantitative basis for this comparison. For R_a, the relaxation coefficient k increases from 0.82 for ZnS to 0.96 for ZnSe, while for R_z the corresponding values are 1.45 and 1.51, respectively. The consistently higher k values for ZnSe indicate a somewhat faster approach toward the limiting roughness state. Moreover, in both materials $k(R_z) > k(R_a)$, showing that high-amplitude topographic features relax more rapidly than the average surface roughness. The larger overall roughness reduction together with the higher relaxation coefficients therefore identifies ZnSe as the more responsive of the two materials in terms of irradiation-induced morphological evolution.

Differences are also evident in the structural evolution. The lattice parameter decreases from 0.54413 to approximately 0.54305 nm in ZnS and from 0.56863 to 0.56811 nm in ZnSe, while the coherent-domain size increases from approximately 20 to 27 nm and from 32 to 37 nm, respectively. However, the significance of these changes should not be assessed solely from their absolute magnitudes, because ZnS and ZnSe have different initial lattice parameters and coherent-domain sizes. More importantly, ZnSe exhibits a comparatively smooth evolution of the structural parameters with fluence, whereas ZnS shows weak non-monotonic variations at intermediate fluences. This difference suggests that the irradiation-induced structural response follows somewhat different relaxation kinetics in the two materials.

The distinct responses of ZnS and ZnSe may originate from differences in their intrinsic lattice and defect properties. Substitution of S by the heavier and larger Se anion results in a larger lattice parameter and different bonding characteristics in ZnSe [1–3]. Differences in defect formation and migration energetics, lattice dynamics, and electron–phonon interactions may consequently influence the relative rates of defect accumulation, redistribution, and annihilation. Previous studies of irradiated II–VI semiconductors have likewise shown that radiation-induced structural evolution is strongly material-dependent and governed by the nature and mobility of the generated defects [6–8, 26–28]. In the absence of direct measurements of defect migration in the present study, however, these microscopic factors should be regarded as plausible contributors to the observed ZnS–ZnSe differences rather than as experimentally established mechanisms.

Differences in electron interaction with the two materials may also contribute to their distinct responses. ZnS and ZnSe differ in density, elemental composition, and electron stopping characteristics; consequently, the spatial distribution of deposited energy and radiation-induced defects is not expected to be identical [24, 28]. Although both materials were irradiated under the same nominal conditions, these material-dependent interaction characteristics may influence the quantitative evolution of their morphological and structural parameters.

Overall, the comparative results reveal a common direction of irradiation-induced evolution in both materials but different relaxation kinetics and magnitudes. ZnSe exhibits a larger reduction in surface roughness, slightly higher phenomenological relaxation coefficients, and a comparatively regular structural evolution, whereas ZnS shows a somewhat weaker and less uniform response. These observations demonstrate that the magnitude and kinetics of irradiation-induced relaxation are material-dependent, while the common trends observed in both crystals are consistent with a shared phenomenological framework of defect-mediated nonequilibrium relaxation.

4.4. Physical interpretation of correlated surface and structural evolution

The correlation analysis presented in Section 3.4 provides an experimental basis for comparing the concurrent surface and structural responses to electron irradiation. In both ZnS and ZnSe, decreasing surface roughness is systematically accompanied by an increase in coherent-domain size and a decrease in the lattice parameter. Thus, three independently determined observables — AFM roughness, coherent-domain size, and lattice parameter — evolve concurrently with increasing electron fluence. Although these correlations do not by themselves establish a unique microscopic mechanism, their systematic character indicates that the morphological and structural responses develop simultaneously under the same irradiation conditions.

The R_a-D and R_z-D relationships show that progressive surface smoothing accompanies enlargement of coherent scattering domains. In ZnS, the decrease in R_a from 191 to 34 nm occurs together with an increase in coherent-domain size from approximately 20 to 27 nm, whereas in ZnSe R_a decreases from 168 to 21 nm while the coherent-domain size increases from approximately 32 to 37 nm. The corresponding R_z correlations exhibit the same tendency. These observations indicate that suppression of surface irregularities proceeds concurrently with increasing structural coherence within the irradiated material. Importantly, this correlation should not be interpreted as evidence that coherent-domain enlargement directly causes surface smoothing, or vice versa; rather, both trends may represent parallel responses of the material to irradiation-induced nonequilibrium processes.

The correlations between roughness and lattice parameter provide a complementary structural relationship. For both materials, decreasing R_a and R_z are accompanied by a reduction of the lattice parameter. Within the investigated fluence range, the lattice parameter a decreases from 0.54413 to approximately 0.54305 nm in ZnS and from 0.56863 to 0.56811 nm in ZnSe. Because no additional diffraction peaks or phase transformations are observed, these relatively small lattice changes are more consistently interpreted as modifications within the existing zinc-blende structure rather than formation of a new crystalline phase. Their concurrent evolution with surface roughness is consistent with progressive relaxation of the irradiated crystal structure.

A plausible microscopic framework for these correlated changes involves the generation and subsequent redistribution of irradiation-induced point defects. Energetic electron–atom interactions can produce vacancies, interstitials, and Frenkel-type defect configurations [9, 16, 24, 25]. Their subsequent redistribution and partial recombination may modify local strain fields and structural coherence, while irradiation-assisted atomic rearrangement in near-surface regions may contribute to the reduction of nonequilibrium topographic features. Within this framework, the AFM and XRD trends can be interpreted as parallel manifestations of irradiation-induced nonequilibrium evolution.

This interpretation is consistent with the conceptual model of radiation-induced defect evolution previously proposed for electron-irradiated ZnS and ZnSe crystals [25]. However, the present experiments do not directly resolve defect migration pathways or establish a causal atomic-scale connection between surface smoothing and bulk structural relaxation. Accordingly, the present results are described in terms of correlated surface and structural evolution rather than a directly demonstrated microscopic coupling mechanism. The microscopic origin of these parallel responses requires further defect-sensitive investigation.

Taken together, the AFM–XRD correlations demonstrate concurrent fluence-dependent changes in surface morphology and structural parameters. The simultaneous decrease in R_a and R_z, enlargement of coherent scattering domains, and variation of the lattice parameter provide evidence of correlated morphological and structural evolution under electron irradiation. The microscopic relationship between these responses remains beyond the scope of the present measurements.

5. Conclusion

In the present work, the evolution of surface morphology and structural parameters in ZnS and ZnSe crystals under high-energy electron irradiation was investigated using a phenomenological modeling approach based on the experimental data obtained within the electron fluence range of $(0-2.5) \cdot 10^{17}$ electrons/cm^2.

Atomic force microscopy revealed pronounced irradiation-induced surface smoothing in both materials. For ZnS, the average roughness R_a decreased from 191 to 34 nm ($\approx$5.6-fold), while R_z decreased from 1929 to 399 nm ($\approx$4.8-fold). In ZnSe, R_a decreased from 168 to 21 nm ($\approx$8-fold) and R_z from 1628 to 219 nm ($\approx$7.4-fold). The experimental roughness evolution was successfully described by a first-order phenomenological relaxation model with high coefficients of determination ($R^2 = 0.984-0.998$), confirming the applicability of the proposed exponential relaxation approach.

X-ray diffraction analysis demonstrated irradiation-induced structural relaxation accompanied by coherent-domain enlargement. The lattice parameter decreased from 0.54413 to 0.54305 nm in ZnS and from 0.56863 to 0.56811 nm in ZnSe, whereas the coherent-domain size increased from 19.88 to 26.68 nm for ZnS and from 32.00 to 37.03 nm for ZnSe. In addition, the size-derived dislocation-density estimate decreased from $25.31 \cdot 10^{10}$ to $14.05 \cdot 10^{10}$ cm^{-2} in ZnS and from $9.77 \cdot 10^{10}$ to $7.29 \cdot 10^{10}$ cm^{-2} in ZnSe, as expected from the corresponding increase in D, while the independently refined lattice microstrain decreased from $7.11 \cdot 10^{-3}$ to $5.29 \cdot 10^{-3}$ and from $4.62 \cdot 10^{-3}$ to $3.99 \cdot 10^{-3}$, respectively.

Correlation analysis revealed that the irradiation-induced reduction in surface roughness occurs concurrently with changes in the bulk structural parameters. These trends demonstrate parallel morphological and structural evolution with increasing electron fluence, without establishing a direct causal relationship between the two responses.

Comparative analysis showed that ZnSe exhibits stronger and more regular relaxation behavior than ZnS, characterized by greater surface smoothing, larger relaxation coefficients, and more monotonic structural evolution, indicating a more pronounced and regular irradiation-induced relaxation response in ZnSe under the investigated conditions.

The main scientific contribution of this work is the quantitative phenomenological comparison of irradiation-induced surface smoothing and structural evolution in ZnS and ZnSe crystals. Unlike previous studies that considered morphological and structural changes separately, the present work analyzes their fluence-dependent correlations within a common experimental framework.

Future work may include quantitative defect-kinetics modeling based on diffusion and rate-equation approaches, atomistic simulations, and complementary Raman spectroscopy, optical absorption, TEM characterization, and density functional theory (DFT) calculations to provide deeper insight into the microscopic mechanisms governing irradiation-induced relaxation.

Acknowledgements

This work was carried out within the framework of the 2026 scientific research program of the Institute of Nuclear Physics of the Uzbekistan Academy of Sciences under the projects entitled "Investigation of the Structure, Dynamics, and Internal Structural Features of Functional Materials, Nanosystems, Geological Objects, and Cultural Heritage Objects" and "Optimization of the Electrophysical and Physicomechanical Properties of $A^{III}B^{V}$ and $A^{II}B^{VI}$ Semiconductor Compounds by Thermoradiation Technology." The authors would like to express their sincere appreciation to the personnel of the unique scientific facility "Elektronika U-003" for their assistance in carrying out the electron irradiation experiments. The authors are also grateful to the staff of the Laboratory of Defects and Phase States Physics and the Laboratory of Radiation Physics and Technology of Solid-State Electronics for their continuous technical support and valuable cooperation during the course of this study.

Author contributions

M. Yu. Tashmetov: Conceptualization, Methodology, Supervision, Writing, Visualization, Reviewing and Editing; B. N. Madaminov: Data curation, Writing, Original draft preparation, Investigation, Software, Validation.

Funding

This research was funded by the Uzbekistan Academy of Sciences within the framework of the 2026 scientific research program of the Institute of Nuclear Physics under the projects entitled "Investigation of the Structure, Dynamics, and Internal Structural Features of Functional Materials, Nanosystems, Geological Objects, and Cultural Heritage Objects" and "Optimization of the Electrophysical and Physicomechanical Properties of $A^{III}B^{V}$ and $A^{II}B^{VI}$ Semiconductor Compounds by Thermoradiation Technology."

Conflicts of interest

The authors declare no conflicts of interest.

References

[1] S. Adachi, Properties of Semiconductor Alloys: Group-IV, III-V and II-VI Semiconductors, John Wiley & Sons, 2009. https://doi.org/10.1002/9780470744383.

[2] R. Triboulet, P. Siffert (Eds.), CdTe and Related Compounds: Physics, Defects, Hetero- and Nano-Structures, Crystal Growth, Surfaces and Applications, Elsevier, 2009.

[3] S. Adachi, T. Taguchi, Optical Properties of ZnSe, Physic Review B 43 (1991) 9569–9577. https://doi.org/10.1103/PhysRevB.43.9569.

[4] D. D. Hile et al., Zinc Selenide Semiconductor: Synthesis, Properties and Applications, Nanoscale Compound Semiconductors and Their Optoelectronics Applications (2022) 67–84. https://doi.org/10.1016/B978-0-12-824062-5.00001-4.

[5] M. Yu. Tashmetov, B. N. Madaminov, N. B. Ismatov, F. K. Khallokov, B. A. Abdikamalov, Structure, Morphology and Properties of ZnS Crystal Irradiated by Electrons of Different Fluences, International Journal of Modern Physics B 39 (2025) 2550103. https://doi.org/10.1142/S0217979225501036.

[6] K. Priya, G. K. Rao, V. K. Ashith, G. Sanjeev, V. P. Verma, V. C. Petwal, J. Dwivedi, The Effect of 8 MeV Electron Beam Irradiation on the Structural, Optical and Photoluminescence Properties of ZnS Thin Films, Ceramics International 45 (2019) 2576–2583. https://doi.org/10.1016/j.ceramint.2018.10.188.

[7] H. D. Dhaygude, S. K. Shinde, M. V. Takale, G. M. Lohar, M. C. Rath, V. J. Fulari, Effect of Electron Irradiation on Structural, Morphological and Photoluminescence Properties of ZnS Thin Films, Ceramics International 42 (2016) 10159–10164. https://doi.org/10.1016/j.ceramint.2016.03.129.

[8] M. Yu. Tashmetov, B. N. Madaminov, Structure and Morphology of Electron-Irradiated ZnSe, Radiation Effects and Defects in Solids 180 (2025) 1931–1942. https://doi.org/10.1080/10420150.2025.2509222.

[9] F. C. Rong, W. A. Barry, J. F. Donegan, G. D. Watkins, Vacancies, Interstitials, and Close Frenkel Pairs on the Zinc Sublattice of ZnSe, Physical Review B 54 (1996) 7779–7788. https://doi.org/10.1103/PhysRevB.54.7779.

[10] G. J. Dienes, A. C. Damask, Radiation Enhanced Diffusion in Solids, Journal of Applied Physics 29 (1958) 1713–1721. https://doi.org/10.1063/1.1723032.

[11] S. G. Mayr, R. S. Averback, Surface Smoothing of Rough Amorphous Films by Irradiation-Induced Viscous Flow, Physical Review Letters 87 (2001) 196106. https://doi.org/10.1103/PhysRevLett.87.196106.

[12] W. W. Mullins, Flattening of a Nearly Plane Solid Surface due to Capillarity, Journal of Applied Physics 30 (1959) 77–83. https://doi.org/10.1063/1.1734979.

[13] H. E. Bennett, J. O. Porteus, Relation between Surface Roughness and Specular Reflection at Normal Incidence, Journal of the Optical Society of America 51 (1961) 123–129. https://doi.org/10.1364/JOSA.51.000123.

[14] B. N. Madaminov, M. Yu. Tashmetov, Influence of High-Fluence Electron Irradiation on the Band Gap, Raman Spectra, and Microhardness of ZnSe, Physica Scripta 100 (2025) 055919. https://doi.org/10.1088/1402-4896/adc6cc.

[15] C. Klingshirn, Semiconductor Optics, 4th ed., Springer, Berlin, Germany, 2012. https://doi.org/10.1007/978-3-642-28362-8.

[16] S. Brunner, W. Puff, A. G. Balogh, P. Mascher, Radiation-Induced Defects in Electron and Proton Irradiated ZnS, Materials Research Society Symposium Proceedings 540 (1998) 213–218. https://doi.org/10.1557/PROC-540-213.

[17] M. Yu. Tashmetov, N. B. Ismatov, R. P. Saidov, Sh. M. Makhkamov, Radiation Treatment Complex on the Base of the Electronics U-003 Electron Accelerator, Problems of Atomic Science and

Technology 5 (2017) 91–94.

[18] M. Yu. Tashmetov, Kh. Djangabaev, Study of Radiation-Induced Effects in GaAs(O):Cr under 2 MeV Electron Irradiation Using Raman, FTIR and Hall Effect Measurements, Physica Scripta 100 (2025) 125918. https://doi.org/10.1088/1402-4896/ae26ef.

[19] J. Rodriguez-Carvajal, FULLPROF: A Program for Rietveld Refinement and Pattern Matching Analysis, Abstracts of the Satellite Meeting on Powder Diffraction of the XV Congress of the IUCr, Toulouse, France, 1990, p. 127.

[20] A. L. Patterson, The Scherrer Formula for X-Ray Particle Size Determination, Physical Review 56 (1939) 978–982. https://doi.org/10.1103/PhysRev.56.978.

[21] M. Tashmetov, A. Abdaminov, K. Djangabaev, O. Tolbanov, N. Ismatov, The Study of Structure, Electrophysical, Physicomechanical and Optical Properties of GaAs with Oxygen Impurities and Doped Chromium, Physica B: Condensed Matter 713 (2025) 417377. https://doi.org/10.1016/j.physb.2025.417377.

[22] G. K. Williamson, R. E. Smallman, Dislocation Densities in Some Annealed and Cold-Worked Metals from Measurements on the X-Ray Debye–Scherrer Spectrum, Philosophical Magazine 1 (1956) 34–46. https://doi.org/10.1080/14786435608238074.

[23] A. R. Stokes, A. J. C. Wilson, The Diffraction of X-Rays by Distorted Crystal Aggregates — I, Proceedings of the Physical Society 56 (1944) 174–181. https://doi.org/10.1088/0959-5309/56/3/303.

[24] G. J. Dienes, G. H. Vineyard, Radiation Effects in Solids, Interscience Publishers, New York, 1957.

[25] M. Yu. Tashmetov, A. V. Belushkin, B. N. Madaminov, M. B. Tagaev, Physical Mechanisms of Structural, Morphological, and Property Changes in ZnS and ZnSe under Electron Irradiation, Journal of Physics: Condensed Matter 38 (2026) 055703. https://doi.org/10.1088/1361-648X/ae3b84.

[26] M. A. Nicolet, Diffusion Barriers in Thin Films, Thin Solid Films 52 (1978) 415–443. https://doi.org/10.1016/0040-6090(78)90184-0.

[27] H. Trinkaus, B. N. Singh, Helium Accumulation in Metals During Irradiation — Where Do We Stand?, Journal of Nuclear Materials 323 (2003) 229–242. https://doi.org/10.1016/j.jnucmat.2003.09.001.

[28] W. Liu, Y. Ji, P. Tan, H. Zang, C. He, D. Yun, C. Zhang, Z. Yang, Irradiation Induced Microstructure Evolution in Nanostructured Materials: A Review, Materials 9 (2016) 105. https://doi.org/10.3390/ma9020105.

[29] M. J. Berger, J. S. Coursey, M. A. Zucker, J. Chang, ESTAR, PSTAR, and ASTAR: Computer Programs for Calculating Stopping-Power and Range Tables for Electrons, Protons, and Helium Ions, NIST Standard Reference Database 124, National Institute of Standards and Technology. https://doi.org/10.18434/T4NC7P.